Mahdi Arian Nik, Larry Lessard and Damiano Pasini*

Size-dependent behavior of laminates with curvilinear fibers made by automated fiber placement

Abstract: Variable stiffness laminates can be manufactured using curvilinear fiber paths. A curvilinear fiber path is generally defined based on the plate size and has a curvature that is dependent on the plate size. In practice, however, the fiber path must satisfy manufacturing constraints, such as the minimum turning radius imposed by the automated fiber placement machine, thereby limiting the possible amount of fiber steering. In this work, we studied the effect of the plate size on the structural properties of a plate manufactured with curvilinear fibers. We considered four plate sizes, which were designed by a constant curvature fiber path. We optimized the plates for both maximum buckling load and in-plane stiffness. The results showed that the in-plane stiffness of the plate was not controlled by the plate size, whereas the buckling load was highly affected by the curvature of the fiber path. Hence, the potential of a buckling load increase reduced for plate sizes smaller than the minimum turning radius. In addition, for a given maximum curvature of the fiber path, the influence of a complex layup on the buckling load was marginal.

Keywords: automated fiber placement; fiber path curvature; gaps and overlaps; multi-objective optimization; size-dependent.

DOI 10.1515/secm-2014-0167
Received May 30, 2014; accepted September 27, 2014

***Corresponding author: Damiano Pasini,** Department of Mechanical Engineering, McGill University, Macdonald Engineering Building, 817 Sherbrooke West, Montreal, QC, H3A 0C3, Canada, e-mail: damiano.pasini@mcgill.ca
Mahdi Arian Nik and Larry Lessard: Department of Mechanical Engineering, McGill University, Macdonald Engineering Building, 817 Sherbrooke West, Montreal, QC, H3A 0C3, Canada

1 Introduction

Automated fiber placement (AFP) is an advanced technology used in aerospace industries to manufacture composite laminates. Thus far, AFP has proven to be capable of producing high quality parts with remarkable accuracy and repeatability. In addition, AFP can manufacture non-traditional composite layups with curvilinear fiber paths, which are referred to as variable stiffness designs. The control of the fiber path orientation gives freedom to tailor the composite properties in directions within the laminate that are more favorable to carry loads. As a result, superior structural performance of a variable stiffness design over a constant stiffness design can be obtained for a range of structural properties, such as buckling resistance [1–4], post-buckling [5–7], fundamental frequency [8–10], and simultaneous maximization of buckling load and in-plane stiffness [11, 12]. In practice, the method used by AFP to manufacture a laminate with curvilinear fibers generally leads to the generation of defects in the form of gaps and overlaps. The reason is that during the manufacturing process, an AFP machine can change the course width only by a discrete value by either adding or dropping tows. Thus, small areas of defects (i.e., either missing or overlaying fibers) would form within the laminate. A method, namely Defect Layer, has been recently introduced [12, 13] to appraise the impact of defects on the performance of variable stiffness composite structures. It has been found that the effect of gaps deteriorates the buckling load and in-plane stiffness of a variable stiffness laminate, whereas the effect of overlaps improves those properties. Croft et al. [14] experimentally explored the effect of gaps and overlaps on the ultimate strengths of constant stiffness laminates. They found that defects along the length of the specimen (0° direction) have a more severe decrease in the mechanical properties than defects along the width of the specimen (90° direction).

Several studies [1–3] reported that the use of a curvilinear fiber path allows transfer of the load from the plate center to the edges, a feature that is highly desirable in raising the buckling resistance of a plate. Thus, on

one hand, variable stiffness laminates that are designed to maximize the buckling load tend to have a fiber path with large curvature [3, 12]. On the other hand, AFP must respect a fiber curvature constraint to prevent the fibers to locally buckle along a curvilinear path. To design a variable stiffness composite plate, a curvilinear fiber path is generally defined as a function of the fiber orientation, which is a variable that changes from the value of T_0 at the plate center to T_1 at a characteristic distance, d, from the plate center. The characteristic distance of d is generally considered to be equal to half the plate width [1, 15]. As a result, the plate size becomes an important factor that affects the curvature of the fiber path, the amount of defects within the laminate, consequently influencing the performance improvement that can be obtained with a variable stiffness design. In this study, the effect of the plate size on the maximum achievable improvements in the buckling load and in-plane stiffness of a variable stiffness plate was investigated. First, the feasible design space of a variable stiffness laminate with a constant curvature fiber path was examined for four plate sizes. The optimum solutions for simultaneous maximization of the buckling load and in-plane stiffness were then obtained. Next, the buckling load and in-plane stiffness of a simple and a complex layup for a variable stiffness laminate were compared. Finally, a discussion of the results follows together with design recommendations.

2 Formulation of the curvilinear fiber path

One way to design a variable stiffness plate is to define a reference path along which the AFP machine places the first course. Subsequent fiber paths can then be obtained by shifting the reference fiber path. As a reference fiber path, a constant curvature path was used here (Figure 1). In the definition of a constant curvature fiber path [15], it is assumed that the path from T_0 (fiber orientation at the plate center) to T_1 (fiber orientation at the plate edges) varies in a way that the radius of the path remains constant. Along this reference path, the fiber orientation can be defined as a function of the plate spatial coordinates given by

$$\theta(x)=\arccos\left(\cos(T_0)+\frac{\cos(T_1)-\cos(T_0)}{a/2}|x|\right), \quad (1)$$

where θ represents the fiber orientation along the fiber path, a is the plate width, and |.| denotes the absolute value. A single layer with this fiber path definition may be represented by $[+<T_0|T_1>]$, where $T_1=T_0$ represents the limiting case of a straight-fiber layer.

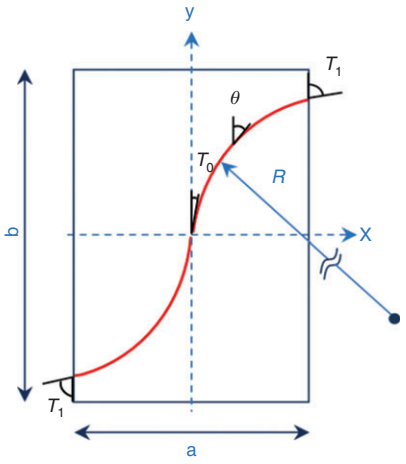

Figure 1 Constant curvature fiber path definition.

The turning radius of the fiber path can be expressed as

$$R=\left|\frac{a/2}{[\cos(T_1)-\cos(T_0)]}\right|. \quad (2)$$

According to Eq. (2), the turning radius of a constant curvature fiber path depends on the plate width, a. A minimum constraint on the turning radius is generally used by an AFP machine so as to avoid local buckling in the fibers placed along a curvilinear path. For a typical AFP machine, the minimum turning radius would be 0.635 m (25 in). When this manufacturing constraint is substituted in Eq. (2), the whole design space (the number of designs $[<T_0|T_1>]$ manufacturable with AFP) for a constant curvature fiber path becomes feasible only for a plate width larger than 1.27 m (50 in). In other words, the number of variable stiffness designs $[<T_0|T_1>]$ manufacturable with AFP is limited for plates with a width that is smaller than the minimum turning radius.

3 Manufacturable design space

To investigate the relation between the size of the feasible design space and the plate size, we considered four plate sizes. The first design was a plate of 0.101×0.152 m (4×6 in), as recommended in the ASTM D7137 standards for compressive strength properties. Given that the ASTM plate size was very small compared to the minimum AFP

turning radius, we selected, as second and third designs, plate sizes of 0.202×0.304 m (8×12 in) and 0.303×0.456 m (12×18 in), which were double and triple the size of the ASTM-recommended plate, respectively. Finally, as a fourth option, a plate size of 0.254×0.406 m (10×16 in), a size used in the industry, was also examined. Figure 2 shows the feasible design spaces (shaded area) with respect to T_0 and T_1 for the selected plate sizes, assuming the minimum turning radius of 0.635 m (25 in.).

As expected, an increase in the plate width resulted in a larger feasible space. For example, only 15% of the whole variable stiffness design space (shaded area in Figure 2A) can be manufactured for the smallest plate size. The percentage of feasible designs increased to 27%, 37%, and 32% for the second, third and fourth plate sizes considered in this work, respectively. In practice, for a very small T_1, the course width at the plate edges becomes too small, and AFP has to drop all the tows within the course before reaching the plate edges [12, 16]. Hence for a constant curvature fiber path, laminates with a very small T_1 are not manufacturable, regardless of the plate size.

To evaluate the impact of plate size on the response of a variable stiffness laminate, we simultaneously maximized the buckling load and in-plane stiffness for each of the plate sizes. As a case study, a 16-ply balanced symmetric $[\pm\theta(x)]_{4s}$ laminate subjected to a uniform end shortening along the y-direction was considered. The optimization problem can be formulated as

$$\begin{aligned} &\min_{\mathbf{x}}\{1/E_{eq}(\mathbf{x}),\ 1/N_{cr}(\mathbf{x})\};\mathbf{x}=(T_0,\ T_1)^T \\ &s.t.\ \{T_0,\ T_1\in[0^\circ,\ 90^\circ]\ \ \&\ \ R_{\min}\geq 0.635m\}, \end{aligned} \tag{3}$$

where $\mathbf{x}$ is the vector of design variables (i.e., T_0 and T_1); E_{eq} and N_{cr} are the equivalent in-plane stiffness and the buckling load of the plate, respectively; and $R_{\min}$ is the minimum turning radius of the fibers over the entire

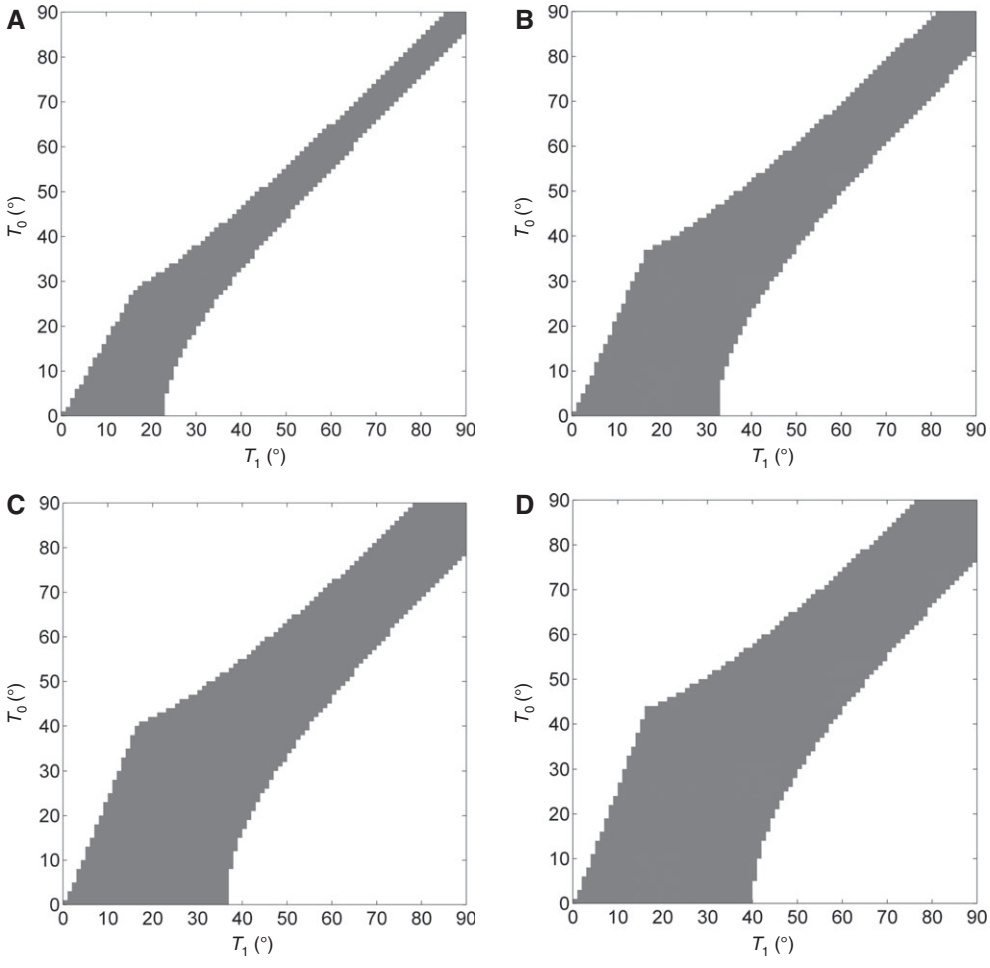

Figure 2 Feasible design space (shaded area) for different plate sizes.
(A) 0.101×0.152 m, (B) 0.203×0.303 m, (C) 0.254×0.406 m, (D) 0.303×0.456.

course width. A comprehensive review of optimization algorithms used in variable stiffness design of composite laminates can be found in [17]. The Genetic algorithm (GA) has been widely used and recommended for optimizing composite structures among several evolutionary optimization algorithms capable of returning a population of solutions at each iteration [17]. However, being a population-based algorithm, GA, requires a large number of function evaluations to reach the optimum solution. This requirement makes the process of finding an optimum design for a variable stiffness composite computationally expensive. The reason for this is that a large computational effort is needed to evaluate the performance of a variable stiffness laminate, especially when the effect of defects within the laminate is accounted for. To overcome this issue, the coupling of an approximation concept, also called a metamodel or surrogate model, with GA has been recognized beneficial [18]. Significantly cheaper to evaluate, the surrogate model is used in place of a high fidelity finite element simulation. As a result, the surrogate model can significantly reduce the time required to run the optimization. In this study, a surrogate-based multi-objective optimization algorithm (NSGAII+RBF) [18] was used to find the Pareto optimal solutions. The radial basis function (RBF) method uses a combination of basis functions expressed in terms of the Euclidean distance between sample data points to construct a surrogate model [19]. The RBF model can be written as

$$\tilde{y}(\mathbf{x}) = \sum_{i=1}^{ns} w_i \psi(\|\mathbf{x}\text{-}\mathbf{x}_i\|), \tag{4}$$

where $\mathbf{x}_i$ (i=1, ..., ns) are the ith data point, ψ is the basis function, and w_i (i=1, ..., ns) are the basis function weights evaluated by fitting the model to the training data; $\|\cdot\|$ denotes the Euclidean distance between two sample data points; and $\tilde{y}$ is the approximate value of the objective function [20]. For a more detailed description of the surrogate-based algorithm, please refer to [11, 18].

The Pareto fronts in Figure 3 showed that the maximum achievable improvement in the buckling load and in-plane stiffness changed with the plate size for a defect-free (ignoring the presence of defects) variable stiffness laminate. The buckling load and in-plane stiffness of the plates were normalized by the corresponding values of a constant stiffness laminate with $[45/0/\text{-}45/90]_{2s}$ (quasi-isotropic) layup. By examining the right portions of the Pareto fronts, we noted that the plate size had no effect on the optimum designs for higher values of the in-plane stiffness. The reason for this trend is that for high in-plane stiffness, the fiber path is closed to the case with straight-fibers, which has a turning

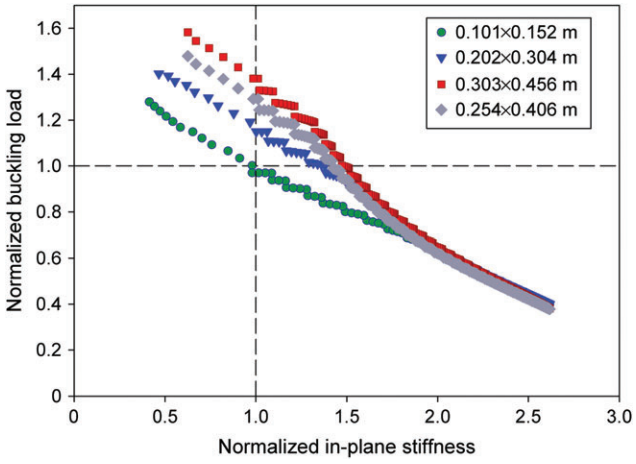

Figure 3 Pareto sets obtained by maximizing the buckling load and in-plane stiffness for four plate sizes.

radius much larger than the minimum allowable turning radius. Meanwhile, the designs that provide a high buckling load tend to have a fiber path with high curvature. As a result, the difference among the three Pareto fronts generally increases with higher values of the buckling load. The largest improvement in the buckling load can be obtained with the largest plate size. It is worth mentioning that for the smallest plate size (0.101×0.152 m), there were no solutions capable of simultaneously improving both the buckling load and in-plane stiffness.

To evaluate the impact of the minimum turning radius, we plotted in Figure 4 the Pareto fronts with and without accounting for the minimum turning constraint in the optimization formulation. The results given for a plate size of 0.254×0.406 m (10×16 in) showed that the constraint on the fiber path curvature had a more pronounced impact

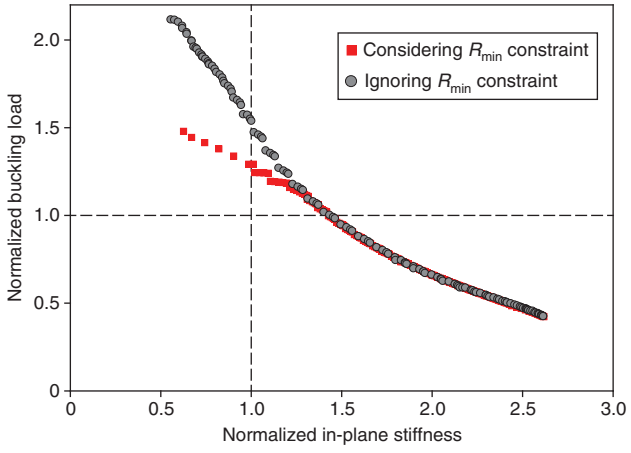

Figure 4 The effect of the minimum turning radius (R_{min}) on the Pareto front for maximum buckling load and in-plane stiffness.

on the solutions with high buckling load than on the baseline. For the unconstrained case, 118% improvement in the buckling load was achieved by the $[\pm<72|0>]_{4s}$ laminate, which had a turning radius of 0.18 m (7.2 in), a value much smaller than the minimum allowable turning radius of a typical AFP machine. Meanwhile, the turning radius constraint resulted in a $[\pm<45|26>]_{4s}$ laminate, which showed 56% improvement in buckling load. We note that a portion of the loss of the improvement in the buckling load may be regained by using a more complex layup, such as $[\pm\theta_1(x)/\pm\theta_2(x)/\pm\theta_3(x)/\pm\theta_4(x)]_s$ instead of $[\pm\theta(x)]_{4s}$.

4 The effect of layup on the performance of a variable stiffness laminate

As mentioned in Section 3, the plate size of 0.254×0.406 m (10×16 in) was small compared with the minimum turning radius (0.635 m) of a typical AFP machine. As a result, the number of manufacturable designs became very limited (Figure 2C). One way to increase the benefit of a variable stiffness design for such a small plate is by designing each layer separately. In other words, using a more complex layup, such as $[\pm\theta_1(x)/\pm\theta_2(x)/\pm\theta_3(x)/\pm\theta_4(x)]_s$ instead of $[\pm\theta(x)]_{4s}$, may result in higher buckling load. Figure 5 compares the Pareto solutions for the $[\pm\theta(x)]_{4s}$ and $[\pm\theta_1(x)/\pm\theta_2(x)/\pm\theta_3(x)/\pm\theta_4(x)]_s$ layups, for a given plate size and maximum curvature of the fiber path. Table 1 summarizes the buckling load and in-plane stiffness of the designs that provide the highest improvement in the buckling load compared with the baseline (quasi-isotropic laminate). In contrast to the $[\pm\theta(x)]_{4s}$ layup, the design that had the highest buckling load for the $[\pm\theta_1(x)/\pm\theta_2(x)/\pm\theta_3(x)/\pm\theta_4(x)]_s$ layup changed with the manufacturing strategy, either with complete gap or overlap (Table 1). The use of a complex layup tailored in each layer of the laminate also increased the maximum improvement in the buckling load of about 5%

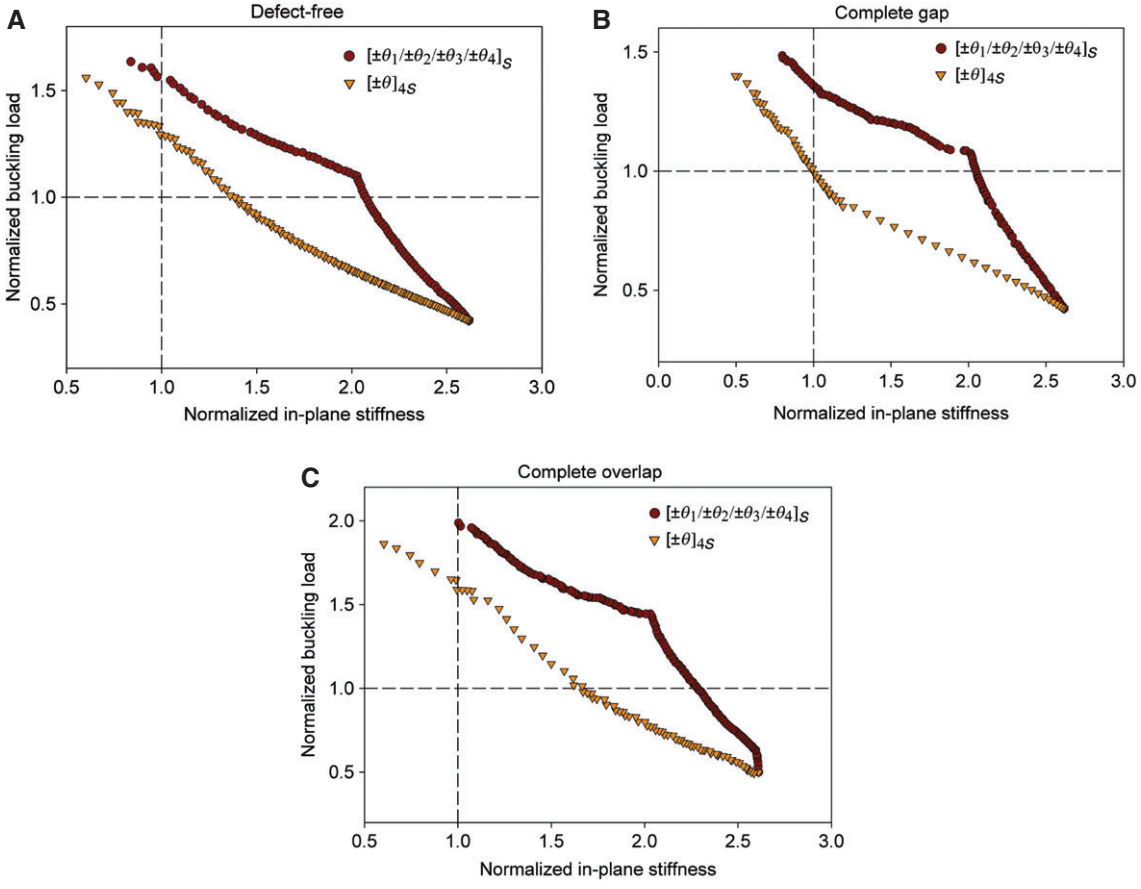

Figure 5 Pareto set obtained by maximizing the buckling load and the in-plane stiffness of a plate with $[\pm\theta(x)]_{4s}$ and $[\pm\theta_1(x)/\pm\theta_2(x)/\pm\theta_3(x)/\pm\theta_4(x)]_s$ layups. (A) Defect-free, (B) Complete gap, (C) Complete overlap.

Table 1 Structural properties of designs with the highest buckling load with $[\pm\theta(x)]_{4s}$ and $[\pm\theta_1(x)/\pm\theta_2(x)/\pm\theta_3(x)/\pm\theta_4(x)]_s$ layups normalized with respect to the baseline.

Case	Layup	Normalized buckling load	Normalized in-plane stiffness
Defect-free	$[\pm<45\|26>]_{4s}$	1.56	0.60
	$[\pm<42\|52>/\pm<43\|22>/\pm<41\|19>/\pm<40\|16>]_s$	1.63	0.84
Complete gap	$[\pm<45\|26>]_{4s}$	1.39	0.52
	$[\pm<44\|44>/\pm<41\|21>/\pm<36\|11>/\pm<37\|11>]_s$	1.46	0.81
Complete overlap	$[\pm<45\|26>]_{4s}$	1.86	0.61
	$[\pm<49\|32>/\pm<41\|19>/\pm<40\|16>/\pm<40\|16>]_s$	1.97	1.06

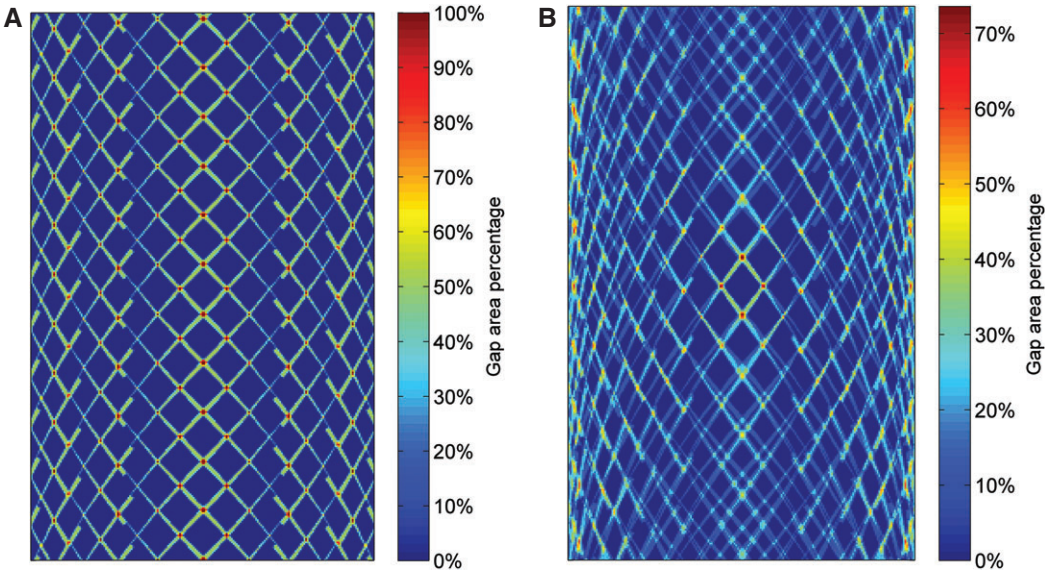

Figure 6 Gap distribution within the laminate averaged through the thickness.
(A) $[\pm<45|26>]_{4s}$, (B) $[\pm<44|44>/\pm<41|21>/\pm<36|11>/\pm<37|11>]_s$.

(Figure 5). Although the use of a complex layup cannot significantly improve the maximum achievable buckling load, we observed a shift of the Pareto front toward higher in-plane stiffness values. This trend indicated that the maximum improvement in the buckling load highly depended on the curvature of the fiber path; hence if the maximum allowable curvature was kept constant, a more complex layup would have had a minor effect on the buckling load. This observation coincides with the findings in Section 3, where the improvement in the buckling load of the laminate was significantly limited by the constraint on the maximum allowable curvature.

The improvement in in-plane stiffness by using the complex layup compared with the simple layup might be attributed to the defect distribution within the laminate. Figure 6 shows the gap distribution for the $[\pm<45|26>]_{4s}$ and $[\pm<44|44>/\pm<41|21>/\pm<36|11>/\pm<37|11>]_s$ layups, which show the highest buckling load for the manufacturing case of a complete gap strategy.

It can be seen that the use of a more complex layup distributed the gap areas within the laminate, as opposed to the case of a simple layup. Furthermore, in the $[\pm<45|26>]_{4s}$ laminate, there were areas with 100% gap, indicating areas that were resin-rich through the whole thickness. For a $[\pm<44|44>/\pm<41|21>/\pm<36|11>/\pm<37|11>]_s$ layup, the maximum gap area percentage through the thickness was about 75%.

5 Conclusions

This work examined the potential improvement in the buckling load for a composite laminate with variable

stiffness. We showed that a plate smaller than twice the minimum AFP turning radius proportionally reduced the number of possible designs that can be manufactured with a constant curvature fiber path. As a result, the performance improvement became marginal. We also found that the plate size did not affect the maximum achievable in-plane stiffness, as opposed to the buckling load, which was highly dependent on the fiber path curvature. Furthermore, the maximum achievable improvement in the buckling load cannot be significantly increased when a more complex layup was used for a given maximum allowable curvature. In comparison, the use of a complex layup shifted the Pareto front towards higher in-plane stiffness values if both buckling load and in-plane stiffness were simultaneously optimized. The results in this paper help gain insight into the advantages and limitations that AFP technology offers for variable stiffness laminate.

The optimized fiber trajectories for the variable stiffness designs were obtained for a specific pair of structural properties, i.e., maximum buckling load and in-plane stiffness. Future research would be required to obtain a Pareto front for various conflicting structural properties, such as failure load, and fundamental frequency that might result in designs with different fiber trajectories.

Acknowledgments: The authors would like to acknowledge the financial support provided by the NSERC-CRD (Grant No. 382132-09) and by the Consortium for Research and Innovation in Aerospace in Québec (CRIAQ). We also thank the support of the National Research Council of Canada, Bombardier Aerospace, and Composites Atlantic.

References

[1] Gürdal Z, Tatting BF, Wu CK. *Composites Part A*. 2008, 39, 911–922.
[2] Lopes C, Gürdal Z, Camanho P. *Comput. Struct*. 2008, 86, 897–907.
[3] Alhajahmad A, Abdalla MM, Gürdal Z. *J. Aircraft* 2010, 47, 775–782.
[4] Raju G, Wu Z, Kim BC, Weaver PM. *Compos. Struct*. 2012, 94, 2961–2970.
[5] Rahman T, Ijsselmuiden ST, Abdalla MM, Jansen EL. *Int. J. Struct. Stab. Dy*. 2011, 11, 735–753.
[6] Raju G, Wu Z, Weaver PM. *Compos. Struct*. 2013, 106, 74–84.
[7] Wu Z, Weaver PM, Raju G. *Compos. Struct*. 2013, 103, 34–42.
[8] Blom A, Setoodeh S, Hol J, Gürdal Z. *Comput. Struct*. 2008, 86, 870–878.
[9] Akhavan H, Ribeiro P. *Compos. Struct*. 2011, 93, 3040–3047.
[10] Ribeiro P, Akhavan H. *Compos. Struct*. 2012, 94, 2424–2432.
[11] Arian Nik M, Fayazbakhsh K, Pasini D, Lessard L. *Compos. Struct*. 2012, 94, 2306–2313.
[12] Arian Nik M, Fayazbakhsh K, Pasini D, Lessard L. *Compos. Struct*. 2014, 107, 160–166.
[13] Fayazbakhsh K, Arian Nik M, Pasini D, Lessard L. *Compos. Struct*. 2013, 97, 245–251.
[14] Croft K, Lessard L, Pasini D, Hojjati M, Chen J, Yousefpour A. *Composites Part A*. 2011, 42, 484–491.
[15] Blom AW, Lopes CS, Kromwijk PJ, Gürdal Z, PP, C. *J. Compos. Mater.* 2009, 43, 403–425.
[16] Falcó O, Mayugo JA, Lopes CS, Gascons N, Turon A, Costa J. *Composites Part B*. 2014, 56, 660–669.
[17] Ghiasi H, Fayazbakhsh K, Pasini D, Lessard L. *Compos. Struct*. 2010, 93, 1–13.
[18] Arian Nik M, Fayazbakhsh K, Pasini D, Lessard L. *Compos. Struct*. 2014, 107, 494–501.
[19] Dyn N, Levin D, Rippa S. *Siam J. Sci. Comput*. 1986, 7, 639–659.
[20] Forrester A, Keane A. *Prog. Aerosp. Sci*. 2009, 45, 50–79.